Radial Temperature Differences During the Melt Spinning of Fibers

KEITH W. HUTCHENSON,* DAN D. EDIE,† and DENNIS M. RIGGS,‡
Department of Chemical Engineering, Clemson University, Clemson, South Carolina 29631

Synopsis

In this investigation, a numerical model was developed to predict the temperature distribution in a fiber during melt spinning. This model uses the implicit Crank–Nicolson method to solve the governing differential equation for the problem. The model was applied to a series of numerical experiments on a liquid crystalline fiber which is melt-spun. These simulations used typical sets of operating conditions to determine the effect of various operating parameters on the predicted radius profile, spinline tension, and temperature distribution. The effects of spinneret capillary diameter, mass flow rate, ambient air temperature, spinning temperature, and elongational viscosity were investigated. The results of the various runs showed that ambient air temperature and mass flow rate had a significant effect on the predicted radius profile, spinline tension, and temperature distribution. The spinning temperature was an important parameter, but its only significant effect was on the spinline tension. Spinneret capillary diameter and elongational viscosity had little effect on the predicted results.

INTRODUCTION

Melt spinning of fibers is a fundamental process in the glass and synthetic fiber industries. This process involves the continuous drawing of liquid filaments to form fibers. Figure 1 shows a schematic diagram of the melt spinning process. Molten glass, plastic, or liquid crystalline material is extruded through the spinneret into ambient air that is below the solidification temperature. In some industrial melt spinning operations, this quenching process is enhanced by blowing the ambient air at right angles to the threadline. This cooling along the spinning path solidifies the molten jet into a solid filament. An area drawdown is generally induced in the melt zone by winding the solidified fiber on a takeup roll at a higher speed than the mean extrusion velocity. Typically, the as-spun filament is subjected to additional processing for property development.

Heat transfer from the molten fiber to the surrounding medium is an important factor in melt spinning. This factor determines the temperature profile in the melt zone, which in turn affects the stress distribution in the as-spun fiber at the point of solidification. In glass and liquid crystalline fibers this residual stress distribution can significantly affect such ultimate physical properties of the fiber as the solid modulus and the extension-to-break ratio.

* Present address: E. I. Dupont de Nemours and Company, Aiken, SC.
† To whom correspondence should be addressed.
‡ Present address: Exxon Enterprises, Fountain Inn, SC.

Journal of Applied Polymer Science, Vol. 29, 3621–3640 (1984)
 CCC 0021-8995/84/113621-20$04.00

Because of the importance of the temperature and stress profiles, a process model is useful for predicting spinline behavior and for investigating the effect of changes in operating conditions (e.g., spinning temperature, mass flow rate, spinneret capillary diameter, etc.) on the properties of the as-spun filament. A number of mathematical models of the melt spinning process have been reported. Denn[1] gives an extensive review of these models. All but two of the models assume that the fiber temperature varies only with axial distance. That is, they assume there is no radial temperature distribution. The two exceptions are reported by Andrews[2] and Matsuo and Kase.[3] Andrews reported a simplified analytical solution for the temperature distribution within the fiber assuming the radius profile is known, and the temperature profile is axisymmetrical.

Matsuo and Kase extended their earlier axial temperature model[4,5] to include both radial and angular variation in the temperature distribution. The radius profile of the fiber is required for this model. Matsuo and Kase estimated this profile by assuming that the theoretically predicted filament radius profile is independent of the radial and angular temperature distribution. With this assumption, the radius profile was estimated by solving the coupled equations of continuity, motion, and energy presented in their previous work[4,5]:

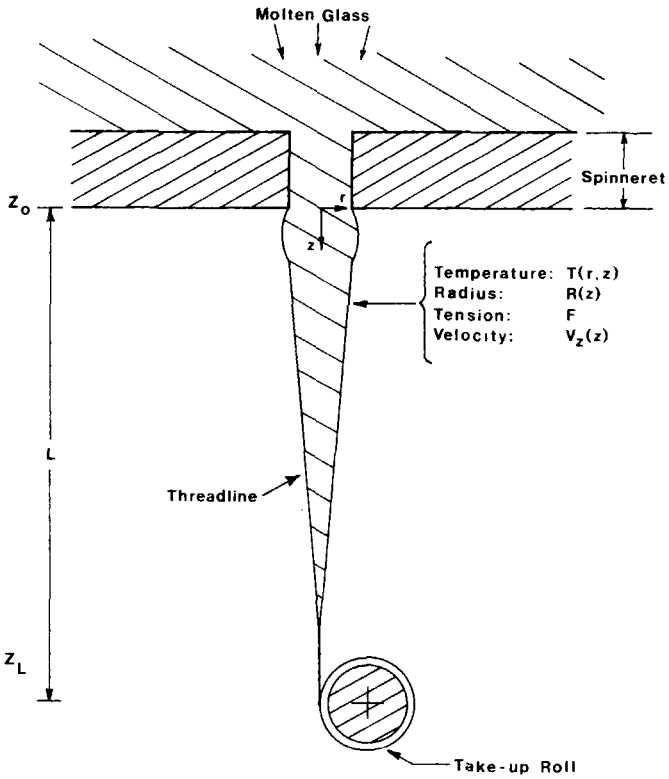

Fig. 1. Schematic diagram of the melt spinning process.

$$\frac{dT}{dz} = -\frac{2(\pi A)^{0.5}\, h\,(T - T_a)}{WC_p} \tag{1}$$

$$\frac{dA}{dz} = -\frac{F\rho}{W\beta} A \tag{2}$$

The heat transfer coefficient h in eq. (1) was given by Kase and Matsuo[4] by the following equation:

$$h = 0.21 k_0 \left(\frac{\pi}{A}\right)^{0.5} \left[\frac{2W}{(\pi A)^{0.5}\rho\nu_0}\right]^{0.334} (1 + C) \tag{3}$$

where C = a corrective coefficient which accounts for the effect of transverse air velocity ($C = 0$ for air flow parallel to the threadline and $C = 1$ for perpendicular air flow). Matsuo and Kase[3] solved the governing differential equation in their model by a modified form of the finite difference method. Half of a circular filament cross section, having a dimensionless radius of unity, was partitioned into 81 arbitrary segments. Each of these segments was assumed to have a uniform temperature. A difference equation was then solved for each segment to step forward incrementally down the fiber.

The purpose of this investigation was to develop a numerical model to estimate the axial and radial temperature distribution in the threadline during melt spinning. The model developed in this investigation uses a more standard numerical method than that of Matsuo and Kase, so that it should be more accurate. The model was then applied to a commercially melt-spun liquid crystalline material which is cooled by air flow parallel to the threadline. The results allowed the determination of the effects of the various operating parameters on the resulting temperature profiles.

DERIVATION OF GOVERNING EQUATION

Assuming (a) steady-state spinning, (b) constant physical properties ρ, C_p, and k, (c) negligible viscous heat dissipation, (d) axisymmetrical flow, (e) axisymmetrical temperature distribution, and (f) negligible axial heat conduction, the equations of continuity and energy[6] for the melt spinning system shown in Figure 1 can be written as

$$\frac{1}{r}\frac{\partial}{\partial r}(rv_r) + \frac{\partial}{\partial z}(v_z) = 0 \tag{4}$$

$$\rho C_p\left[v_r\frac{\partial T}{\partial r} + v_z\frac{\partial T}{\partial z}\right] = k\left[\frac{1}{r}\frac{\partial}{\partial r}\mathrm{r}\frac{\partial T}{\partial r}\right] \tag{5}$$

Assuming that the product (rv_r) is a function of r only, and v_z is a function of z only, eq. (4) can be integrated to give

$$v_r = -\frac{r}{2}\frac{d}{dz}(v_z) \tag{6}$$

The total mass flow rate W is constant and is given by the equation

$$W = \rho A v_z = \rho \pi R^2 v_z \tag{7}$$

Substituting eqs. (6) and (7) into eq. (5), the governing equation of energy reduces to

$$\frac{WC_p}{\pi R^2}\left[\frac{r}{R}\frac{dR}{dz}\frac{\partial T}{\partial r} + \frac{\partial T}{\partial z}\right] = k\left[\frac{\partial^2 T}{\partial r^2} + \frac{1}{r}\frac{\partial T}{\partial r}\right] \tag{8}$$

Equation (8) is the equation of energy governing the temperature distribution in a melt spinning fiber. The solution of this equation requires the availability of the threadline radius as a function of axial distance below the spinneret. This profile can be estimated by making the same assumption as Matsuo and Kase[3] in their model. That is, the radius profile can be calculated by assuming that the theoretically predicted filament radius profile is independent of the radial temperature distribution. With this assumption, the radius profile can be approximated by solving the coupled ordinary differential equations (1) and (2).

Equation (8) can be simplified by expressing it in terms of dimensionless variables. This makes the solution mathematically more general and, as will be seen, numerically easier to solve. The dimensionless radial and axial coordinates, respectively, are defined by

$$\xi = \frac{r}{R(z)} \tag{9}$$

$$\zeta = \frac{kz}{\rho C_p v_z R^2} = \frac{\pi kz}{WC_p} \tag{10}$$

The dimensionless radius defined in eq. (9) varies from 0 to 1 at any given axial position. By reducing the governing equation with this dimensionless variable, the numerical solution of the resulting equation is simplified, since the equation is solved in an even, regular domain. Note that the dimensionless axial coordinate defined in eq. (10) is essentially a pseudo-time variable and can be treated as such in the numerical solution of the final equation. The temperature can be expressed in terms of a dimensionless variable by

$$\theta = \frac{T - T_a}{T_{\text{spin}} - T_a} \tag{11}$$

The functional dependence of the dependent variable T is given by $T = T(r,z)$. Since z is not a function of ξ,

$$\frac{\partial T}{\partial \xi} = \frac{\partial T}{\partial r}\frac{\partial r}{\partial \xi} \tag{12}$$

Substituting for $(\partial r/\partial \xi)$ by eq. (9), we obtain

$$\frac{\partial T}{\partial \xi} = \frac{\partial T}{\partial r}(R) \tag{13}$$

Differentiating with respect to ξ, we obtain

$$\begin{aligned}\frac{\partial^2 T}{\partial \xi^2} &= \frac{\partial}{\partial \xi}\left(\frac{\partial T}{\partial \xi}\right) \\ &= \frac{\partial}{\partial (r/R)}\left(R\frac{\partial T}{\partial r}\right) \\ &= \mathrm{R}^2 \frac{\partial^2 \mathrm{T}}{\partial \mathrm{r}^2}\end{aligned} \tag{14}$$

Also, since T is a function of r and z, we find that

$$\frac{\partial T}{\partial \zeta} = \frac{\partial T}{\partial r}\frac{\partial r}{\partial \zeta} + \frac{\partial T}{\partial z}\frac{\partial z}{\partial \zeta}$$

Substituting for $(\partial r/\partial \zeta)$, $(\partial z/\partial \zeta)$, and $(\partial T/\partial r)$ by eqs. (9), (10), and (13), respectively, we obtain

$$\frac{\partial T}{\partial \zeta} = \frac{\xi}{R}\frac{\mathrm{d}R}{\mathrm{d}\zeta}\frac{\partial T}{\partial \xi} + \frac{\partial T}{\partial \mathrm{z}}\frac{WC_p}{\pi k} \tag{15}$$

Substituting for $(\partial T/\partial z)$, $(\partial T/\partial r)$, and $(\partial^2 T/\partial r^2)$ in eq. (8) by eqs. (13), (14), and (15), respectively, and substituting for the temperature T in terms of the dimensionless variable θ, as given in eq. 11),

$$\frac{\xi}{R}\frac{\mathrm{d}R}{\mathrm{d}\zeta}\frac{\partial \theta}{\partial \xi} + \frac{\partial \theta}{\partial \zeta} = \frac{\partial^2 \theta}{\partial \xi^2} + \left[\frac{\xi}{R}\frac{\mathrm{d}R}{\mathrm{d}\zeta} + \frac{1}{\xi}\right]\frac{\partial \theta}{\partial \xi} \tag{16}$$

or

$$\frac{\partial \theta}{\partial \zeta} = \frac{\partial^2 \theta}{\partial \xi^2} + \frac{1}{\xi}\frac{\partial \theta}{\partial \xi} \tag{17}$$

This is the final form of the governing differential equation for the numerical model. Note that the radial convection term cancels with one of the radial conduction terms.

BOUNDARY CONDITIONS

The following boundary conditions were assumed for the solution of eq. (17):

1. The temperature of the melt at the spinneret face is constant and is

equal to the spinning temperature. Expressing this mathematically in terms of the dimensionless variables, we obtain

$$\theta(\xi,0) = 1.0 \tag{18}$$

2. The radial temperature gradient is zero at the center of the filament. That is,

$$\frac{\partial T}{\partial r} = 0 \text{ at } r = 0$$

or, in dimensionless terms,

$$\frac{\partial}{\partial \xi}\theta(0,\zeta) = 0.0 \tag{19}$$

3. Heat loss from the fiber surface is by convection. This is expressed mathematically by

$$-\frac{\partial T}{\partial r} = \frac{h}{k}(T - T_a) \text{ at } r = R$$

or, in terms of dimensionless variables,

$$\frac{\partial}{\partial \xi}\theta(1,\zeta) = -\left(\frac{hR}{k}\right)\theta \tag{20}$$

The expression for the heat transfer coefficient h given by Kase and Matsuo[4] in eq. (3) was used in this model. Note that the radius profile of the fiber is required in applying this boundary condition.

NUMERICAL SOLUTION TECHNIQUE

As stated previously, the radius profile of the fiber is required to solve eq. (17). The physical shape of the fiber was estimated in this investigation by solving eqs. (1) and (2) for the radius profile by a simultaneous fourth-order Runge–Kutta technique. This radius profile was then used in a finite difference solution of eq. (17). The implicit Crank–Nicolson method[7] was applied to solve this equation. This is a standard numerical technique, and so it should give a more accurate solution than that used by Matsuo and Kase.[3]

The finite difference grid used to model a melt spinning fiber covered the domain $0 \leq \xi \leq 1$ and $\zeta \geq 0$. At any given axial position ζ, there are L radial grid points with $i = 1$ being at the center of the fiber and $i = L$ being at the surface. Subscript (n) represents known values of the dependent variable at a given axial (or time) position, and subscript $(n + 1)$ denotes unknown values at the next axial position. The finite difference equations presented below are then solved at each axial position to step forward incrementally down the fiber. An error analysis to determine the magnitude

of the truncation error in the finite difference analogs indicated that step sizes of $\Delta\xi = 0.025$ and $\Delta\zeta = 0.001$ were sufficient to give negligible error.

Recognizing that ζ is essentially a pseudo-time variable, boundary condition (1) can be treated as an initial condition. Thus, for all radial grid points i,

$$\theta_{i,n=1} = 1.0 \tag{21}$$

The finite difference equation for the interior grid points is given by

$$A_i\theta_{i-1,n+1} + B_i\theta_{i,n+1} + C_i\theta_{i+1,n+1} = D_i \tag{22}$$

where

$$A_i = \left[i - \frac{3}{2} \right]$$

$$B_i = \left[-\frac{2(i-1)(\Delta\xi)^2}{\Delta\zeta} - 2(i-1) \right]$$

$$C_i = \left[i - \frac{1}{2} \right]$$

$$D_i = \left[-i + \frac{3}{2} \right]\theta_{i-1,n} + \left[-\frac{2(i-1)(\Delta\xi)^2}{\Delta\zeta} + 2(i-1) \right]\theta_{i,n} + \left[-i + \frac{1}{2} \right]\theta_{i+1,n}$$

For the center grid point ($i = 1$), the finite difference equation is

$$B_1\theta_{1,n+1} + C_1\theta_{2,n+1} = D_1 \tag{23}$$

where

$$B_1 = \left[-2 - \frac{(\Delta\xi)^2}{(\Delta\zeta)} \right]$$

$$C_1 = [2]$$

$$D_1 = \left[2 - \frac{(\Delta\xi)^2}{(\Delta\zeta)} \right]\theta_{1,n} + [-2]\,\theta_{2,n}$$

The finite difference equation for the surface grid point ($i = L$) is

$$A_L\theta_{L-1,n+1} + B_L\theta_{L,n+1} = D_L \tag{24}$$

where

$$A_L = [2]$$

$$B_L = \left[-\frac{2(\Delta\xi)^2}{\Delta\zeta} - 2 - 2\left(\frac{hR}{k}\right)(\Delta\xi) - \left(\frac{hR}{k}\right)(\Delta\zeta)^2 \right]$$

$$D_L = [-2]\,\theta_{L-1,n} + \left[-\frac{2(\Delta\xi)^2}{\Delta\zeta} + 2 + 2\left(\frac{hR}{k}\right)(\Delta\xi) + \left(\frac{hR}{k}\right)(\Delta\xi)^2\right]\theta_{L,n}$$

RESULTS AND DISCUSSION

A series of numerical experiments was devised to study the predicted radius and temperature profiles for typical sets of operating conditions and to determine what effect various operating parameters have on these profiles. Table I shows the required input data for these runs. Run no. 1 shows the base case used in the analysis. The input data for this run are for "normal" operating conditions. From this base case, the effects of spinneret capillary diameter (runs 2 and 3), mass flow rate (runs 4, 5, and 6), ambient air temperature (runs 7 and 8), spinning temperature (runs 9 and 10), and elongational viscosity (runs 11 and 12) were investigated.

Base Case

Figure 2 shows the predicted filament radius profile for run no. 1. The indicated solidification point was taken as the axial position where the temperature of the center of the fiber reaches a value at or below the glass transition temperature. Note that, although the total distance required for the fiber to reach the solidification point is 0.0359 m, the drawdown is essentially 99% complete at an axial distance of only 0.00684 m. Thus, the drawdown region is small for this material.

Figure 3 displays the radial temperature distribution in the fiber at several axial positions. The initial temperature at $z = 0.0$ m (i.e., at the spinneret face) is the spinning temperature. The temperature across the fiber then decreases as shown as the numerical solution steps forward incrementally down the fiber. Note that the parameter plotted as the abscissa of this graph is the dimensionless radial coordinate defined in eq. (9). This explains the similar shape of the different curves. Plotting the fiber temperature as a function of ξ instead of r tends to dampen the steeper gradients.

Figure 4 shows the center-line surface temperatures of the fiber for run no. 1. At a given axial position, the vertical distance between these two curves represents the radial temperature difference across the fiber. For this base case, the maximum value of the radial temperature difference is 10.106 K. This maximum occurs at an axial distance of 0.00702 m. The radial temperature difference at the solidification point is 4.776 K.

Figures 5 and 6 show isotherms across the fiber near the spinneret face and near the point of maximum radial temperature difference, respectively. Note the steep rate of radius draw-down in Figure 5. The isotherms near the surface follow the radius profile closely in this initial section. The isotherms become flatter as the center of the fiber is approached. This indicates that convective heat loss is the dominant heat transfer mechanism near the spinneret. Heat conduction across the fiber becomes more impor-

TABLE I
Input Data for Simulation Runs[a]

Run No.	Spinnerette capillary diameter (m) × 10^6	Mass flow rate (kg/s) × 10^6	Takeup velocity (m/s)	Ambient air temperature (K)	Spinning temperature (K)	Elongational viscosity constants[b]	
						A_1 (Pa · s)	B_1 (K)
1	200	1.333	8.3577	433.15	630.15	1.17906×10^{-24}	37261.7
2	150	1.333	8.3577	433.15	630.15	1.17906×10^{-24}	37261.7
3	250	1.333	8.3577	433.15	630.15	1.17906×10^{-24}	37261.7
4	200	0.667	4.1788	433.15	630.15	1.17906×10^{-24}	37261.7
5	200	1.000	6.2683	433.15	630.15	1.17906×10^{-24}	37261.7
6	200	1.667	10.4471	433.15	630.15	1.17906×10^{-24}	37261.7
7	200	1.333	8.3577	393.15	630.15	1.17906×10^{-24}	37261.7
8	200	1.333	8.3577	473.15	630.15	1.17906×10^{-24}	37261.7
9	200	1.333	8.3577	433.15	623.15	1.17906×10^{-24}	37261.7
10	200	1.333	8.3577	433.15	638.15	1.17906×10^{-24}	37261.7
11	200	1.333	8.3577	433.15	630.15	1.75539×10^{-29}	44156.7
12	200	1.333	8.3577	433.15	630.15	1.25236×10^{-21}	32888.6

[a] Constant physical properties: specific heat = 1883.7 J/kg · K, density = 1300.0 kg/m^3, thermal conductivity = 0.090 W/m · K, glass transition temperature = 511.15 K.

[b] $\beta = 3A_1 \exp(B_1/T)$

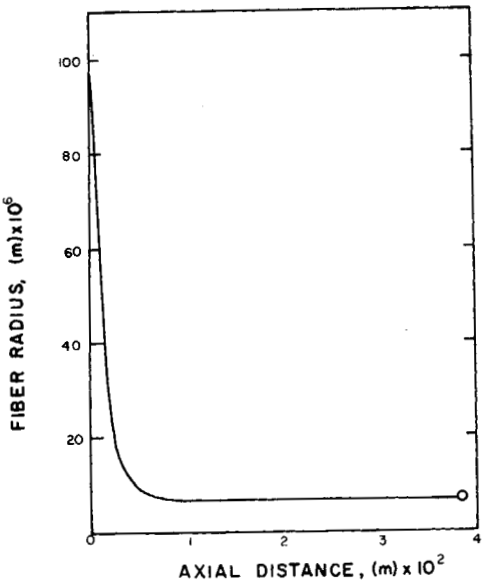

Fig. 2. Radius profile of fiber for run no. 1.

tant as the axial distance increases. The rate of drawdown is substantially smaller in Figure 6 than in Figure 5. The isotherms are flatter and have similar shapes from one temperature to the next. This indicates that, by this point, the radial conduction effect is significant when compared with the convective heat loss effect. For both cases, the radial temperature gradient is steeper near the fiber surface. Thus, convective losses dominate near the surface.

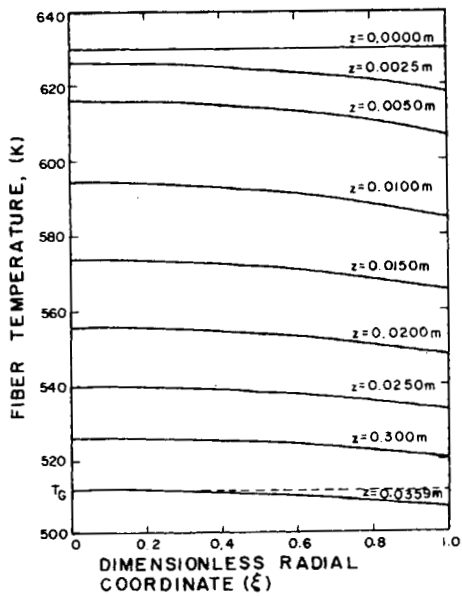

Fig. 3. Temperature distribution at several axial positions for run no. 1.

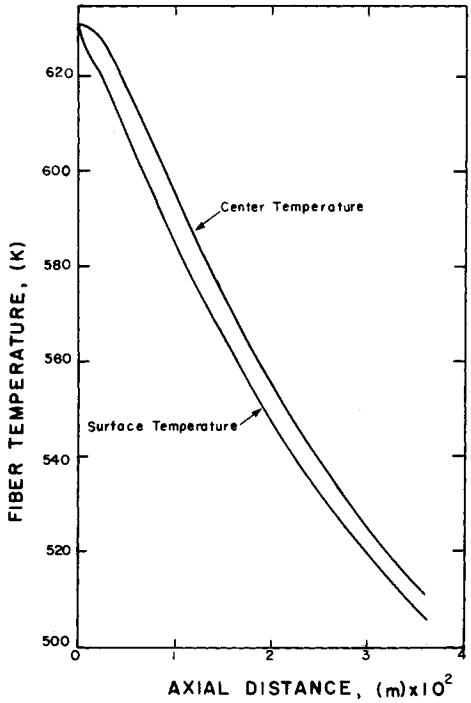

Fig. 4. Axial temperature distribution for run no. 1.

Effect of Various Parameters

Table II shows the calculated spinning tension, maximum radial temperature difference, and the solidification point for the 12 runs given in Table I. Table III shows the effects of changing the various operating parameters on the spinline tension and maximum radial temperature difference. The spinline tension is increased from the base case by increasing

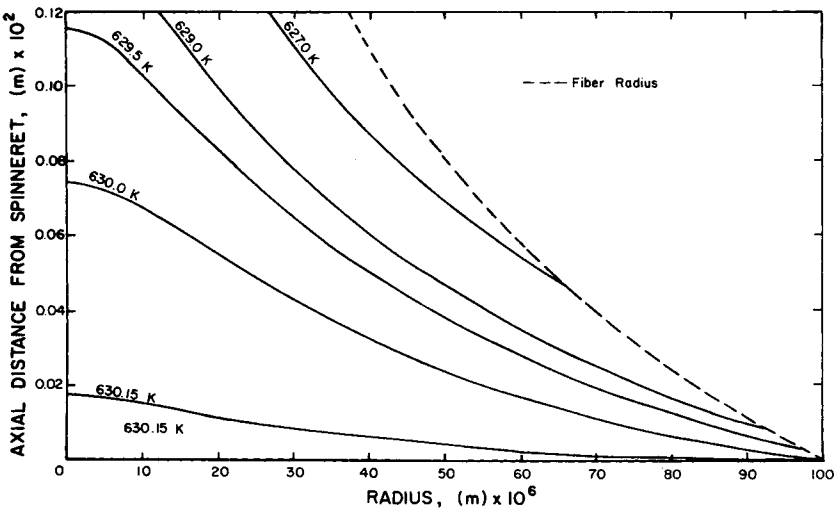

Fig. 5. Isotherms near spinneret face for run no. 1.

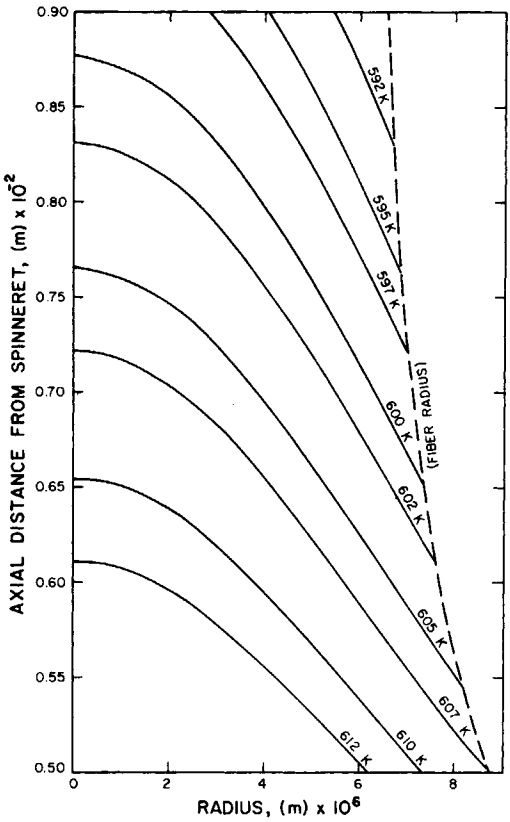

Fig. 6. Isotherms near Point of Maximum Radial Temperature Difference for run no. 1.

the spinneret capillary diameter and throughput and by decreasing the ambient air temperature, spinning temperature, and elongational viscosity. The biggest effect on the spinline tension results from changing the spinning temperature. A decrease in T_{spin} of only 7 K increases the tension by over 91%. Ambient air temperature and throughput also have a significant effect

TABLE II
Overall Results of Simulation Runs

Run no.	Spinline tension (N) × 10^4	Maximum radial temperature difference (K)	Solidification point (m) × 10^2
1	3.280	10.106	3.595
2	3.063	10.146	3.576
3	3.434	10.079	3.610
4	2.602	8.072	2.218
5	2.979	9.208	2.953
6	3.534	10.862	4.191
7	3.865	12.106	2.829
8	2.650	7.988	5.257
9	6.277	9.726	3.472
10	1.588	10.540	3.739
11	3.281	10.329	3.566
12	2.968	9.927	3.621

TABLE III

Effects of Changing the Various Operating Parameters on the Spinline Tension and Maximum Radial Temperature Difference

Run No.	Variable changed	Change in variable	% Change in variable	Change in spinline tension (N) × 10^4	% Change in spinline tension	Change in max. radial temp difference (K)	% Change in maximum radial temp difference
2	D_{spin}	−0.000050 m	−25.0	−0.217	−6.6	+0.040	+0.40
3	D_{spin}	+0.000050 m	+25.0	+0.154	+4.7	−0.027	−0.27
4	W	-0.666×10^{-6} kg/s	−50.0	−0.678	−20.7	−2.034	−20.1
5	W	-0.333×10^{-6} kg/s	−25.0	−0.301	−9.2	−0.898	−8.9
6	W	$+0.334 \times 10^{-6}$ kg/s	+25.0	+0.253	+7.7	+0.756	+7.5
7	T_a	−40 K	−9.2	+0.585	+17.8	+2.000	+19.8
8	T_a	+40 K	+9.2	−0.630	−19.2	−2.118	−21.0
9	T_{spin}	−7 K	−1.1	+2.997	+91.4	−0.380	−3.8
10	T_{spin}	+8 K	+1.3	−1.692	−51.6	+0.434	+4.3
11	β	−26.9 Pa · s[a]	−15.6	+0.001	+0.03	+0.223	+2.2
12	β	+4.64 Pa · s[a]	+2.7	−0.312	−9.5	−0.179	−1.8

[a] Evaluated at 630 K.

on spinline tension. The maximum radial temperature difference is increased by increasing the throughput and spinning temperature and by decreasing the spinneret capillary diameter, ambient air temperature, and elongational viscosity. The parameters that affect the maximum radial temperature difference to the greatest extent are the throughput and ambient air temperature. For example, a 9.2% increase in the ambient air temperature decreases the maximum radial temperature difference by 21%. The axial distance required for solidification is increased by increasing all the parameters studied.

Spinneret Capillary Diameter. Figures 7 and 8 show the effect of spinneret capillary diameter (runs 1, 2, and 3) on the predicted filament radius profile and the radial temperature difference, respectively. The differences in the predicted fiber radii appear to be only a function of the differences in the starting points. The axial distance required for the fiber to reach essentially complete drawdown is approximately the same for the three capillary diameters studied. There is little difference in the radial temperature difference at any axial position. The maximum radial temperature difference is approximately 10.1 K and occurs at roughly the same axial position for all three cases. In addition, as shown in Tables II and III, the solidification point is about the same and there is only a modest effect on the spinline tension. Thus, capillary diameter has little effect on spinline behavior.

Mass Flow Rate. Figures 9 and 10 show the effect of throughput (runs 1, 4, 5, and 6) on the radius profile and the radial temperature difference of the fiber, respectively. Throughput has a significant effect on both of these results. For lower throughputs, the fiber necks down faster and reaches its final radius sooner than for higher throughputs. Also, the maximum radial temperature difference is lower for smaller throughputs. The value of this maximum ranges from 8.072 to 10.862 K for the four cases. The

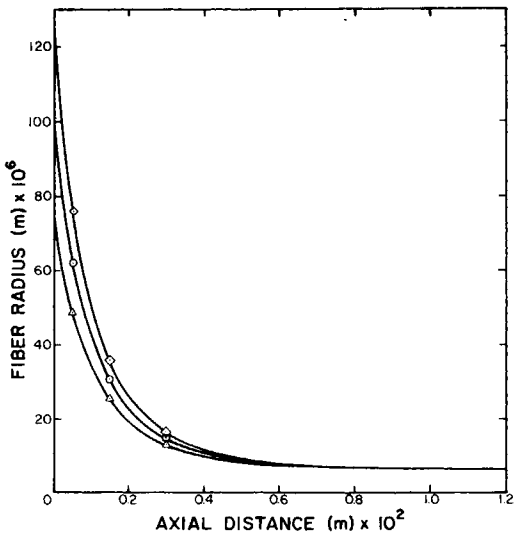

Fig. 7. Effect of spinneret capillary diameter on fiber radius. Spinneret diameter (m): (△) 0.000150; (○) 0.000200; (◇) 0.000250.

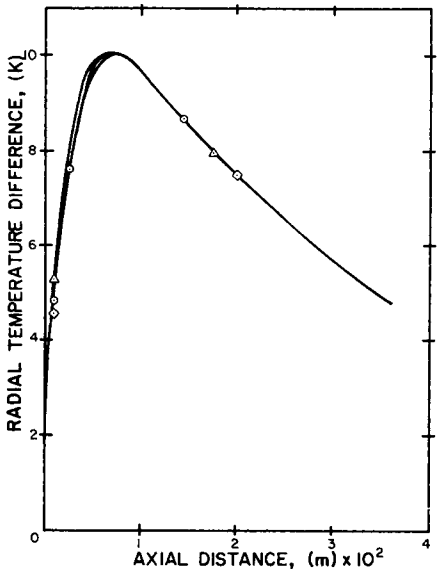

Fig. 8. Effect of spinneret capillary diameter on the radial temperature difference. D_{spin} (m): (△) 0.000150; (⊙) 0.000200; (◇) 0.000250.

axial position of the maximum radial temperature difference is shifted further from the spinneret with increasing mass flow rate. The solidification point increases significantly with increasing throughput, and there is a pronounced effect of throughput on spinline tension. Thus, mass flow rate has a significant effect on fiber characteristics.

Ambient Air Temperature. There is little effect of ambient air temperature (runs 1, 7, and 8) on the radius profile. However, at lower ambient air temperatures, the fiber necks down faster and reaches its final radius sooner than for higher air temperatures. Figure 11 shows the effect of

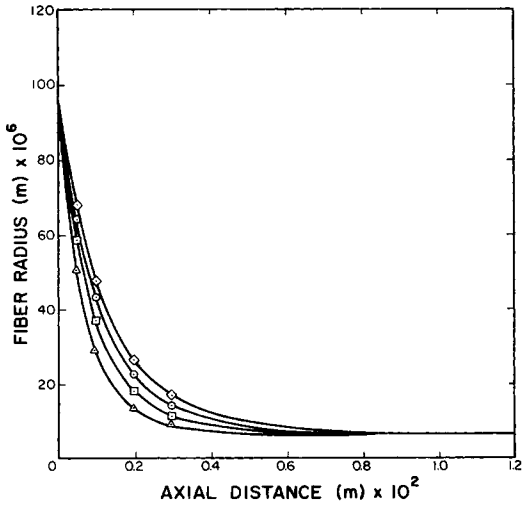

Fig. 9. Effect of throughput on fiber radius. $W(\times 10^{-6}$ kg/s): (△) 0.667; (⊡) 1.000; (⊙) 1.333; (◇) 1.667.

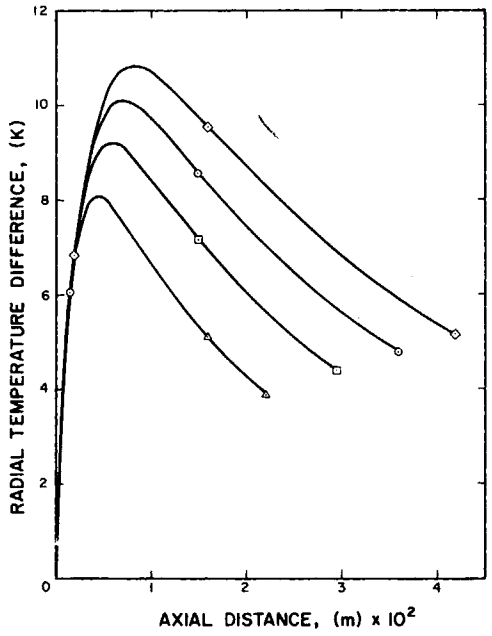

Fig. 10. Effect of throughput on the radial temperature difference. W ($\times 10^{-6}$ kg/s): (△) 0.667; (□) 1.000; (○) 1.333; (◇) 1.666.

ambient air temperature on the radial temperature difference. The maximum radial temperature difference increases appreciably with decreasing air temperatures. This maximum ranges from 7.988 to 12.106 K for ambient air temperatures of 473.15 to 393.15 K, respectively. As shown in Table III, there is a significant effect of ambient air temperature on spinline tension.

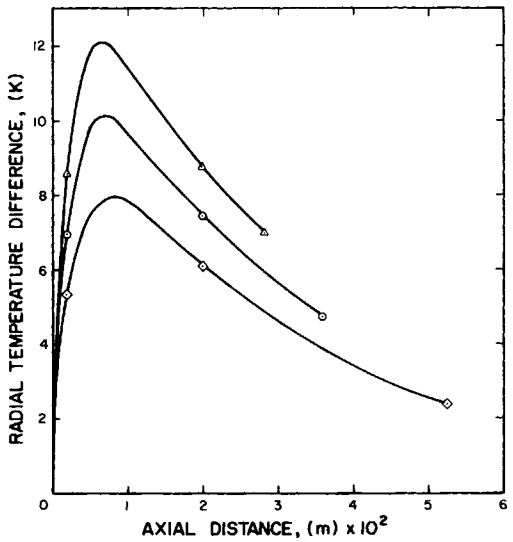

Fig. 11. Effect of ambient air temperature on the radial temperature difference. T_a (K): (△) 393.15; (○) 433.15; (◇)473.15.

Thus, ambient air temperature is an important parameter affecting spinline behavior.

Spinning Temperature. Figure 12 illustrates the effect of spinning temperature (runs 1, 9, and 10) on the radial temperature difference. There is essentially no difference in the filament radius profile for the three cases studied. There is little difference in the radial temperature difference for these runs. The maximum radial temperature difference only ranges from 9.726 to 10.540 K for the three spinning temperatures. The effect of spinning temperature on the spinline tension is significant, however. This was discussed previously.

Elongational Viscosity. Figures 13 and 14 show the effect of elongational viscosity (runs 1, 11, and 12) on the fiber radius and radial temperature difference, respectively. As can be seen from these figures and Tables II and III, the elongational viscosity does not have a pronounced effect on any of the results shown. The biggest effect is seen in the radius profile and spinline tension. For lower viscosities, the fiber necks down faster and the spinline tension is greater. However, these effects are not significant when compared with the effects of some of the other parameters.

Comparison of Effects of Various Parameters

Based on the results presented in this section, mass flow rate and ambient air temperature have the biggest effect on the filament radius profile and the radial temperature distribution (and, thus, the residual stress in the fiber) of the variables studied. These parameters also have a significant influence on the spinline tension. For example, a 50% decrease in the mass flow rate causes a 20.1% decrease in the maximum radial temperature difference and a 20.7% decrease in the spinline tension. A 9.2% increase

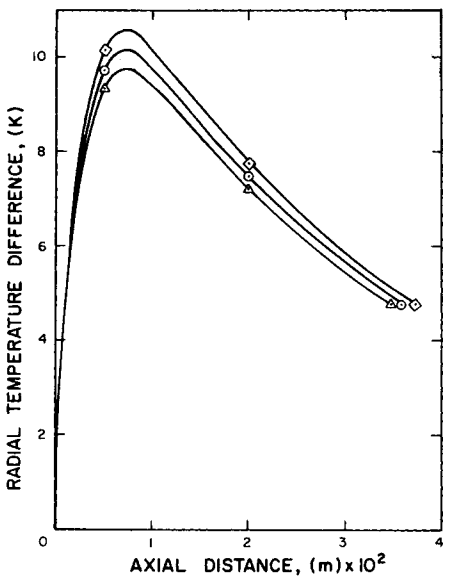

Fig. 12. Effect of spinning temperature on the radial temperature difference. T_{spin} (K): (△) 623.15; (○) 630.15; (◇) 638.15.

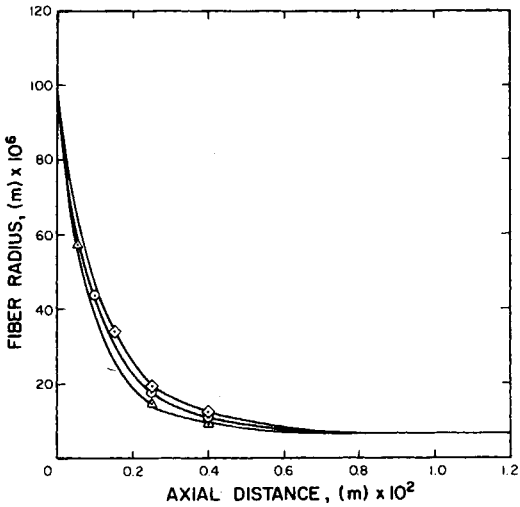

Fig. 13. Effect of elongational viscosity on fiber radius. β: (△) $5.265 \times 10^{-29}\ e^{(44157/T)}$; (⊙) $3.537 \times 10^{-24}\ e^{(37262/T)}$; (◇) $3.756 \times 10^{-21}\ e^{(32889/T)}$.

in the ambient air temperature produces a 21.0% decrease in the maximum radial temperature difference and a 19.2% decrease in the spinline tension. The spinning temperature is also important, but its only significant effect is seen in the spinline tension. A 1.1% decrease in the spinning temperature increases the spinline tension by 91.4% but only causes a 3.8% decrease in the maximum radial temperature difference. Thus, the spinning temperature strongly influences stresses during spinning, while throughput and ambient air temperature have more of an effect on residual stresses.

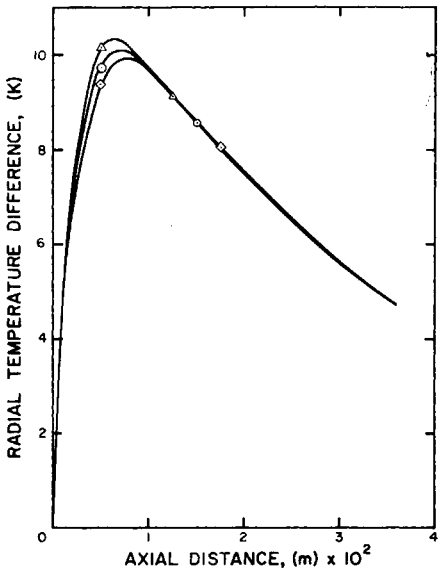

Fig. 14. Effect of elongational viscosity on the radial temperature difference. β: (△) $5.265 \times 10^{-29}\ e^{(44157/T)}$; (⊙) $3.537 \times 10^{-24}\ e^{(37262/T)}$; (◇) $3.756 \times 10^{-21}\ e^{(32889/T)}$.

The spinneret capillary diameter and elongational viscosity have only a slight effect on spinline behavior. For example, a 25% increase in the capillary diameter only causes a 4.7% increase in the spinline tension and a 0.27% decrease in the maximum radial temperature difference. A 15.6% decrease in the elongational viscosity produces a 0.03% increase in the spinline tension and a 2.2% increase in the maximum radial temperature difference. Thus, spinneret capillary diameter and elongational viscosity have only a minimal effect on the residual stress in the fiber. The small effect of elongational viscosity indicates that the momentum equation is less important than the energy equation in modeling this system. The capillary diameter was expected to have a bigger influence on the filament radius profile, the radial temperature difference, and, thus, the residual stress in the fiber. Apparently, the high drawdown rate for the material studied tends to dampen the effect of capillary diameter.

Validity of Model

There is no direct means of experimental verification of the model for the temperature distribution in the fiber. However, based on the results of this investigation, it is believed that the model can give reasonable quantitative estimates of the temperature distribution in a melt spinning fiber. The model should prove especially useful for qualitatively studying trends in the predicted spinline behavior induced by changes in the physical properties of the material being spun or in the actual melt spinning conditions.

SUMMARY

In this investigation, an attempt was made to numerically predict the temperature distribution within a melt spinning fiber. The implicit Crank–Nicolson method was used in the numerical solution of the governing differential equation. The model was applied to a series of numerical experiments to study the effect of various operating parameters on the resulting profiles. The results showed that the numerical model can be used to indicate key variables in the melt spinning process.

For the material studied, mass flow rate and ambient air temperature are key operating variables in determining the radial temperature distribution and, thus, the residual stresses within the fiber. Spinning temperature greatly influences the spinline tension. Spinneret capillary diameter and elongational viscosity have little effect on either radial temperature differences and residual stresses or on spinline tension.

APPENDIX: NOMENCLATURE

A	cross-sectional area of the threadline (m^2)
C_p	isobaric heat capacity of the fiber (J/kg · K)
F	axial tension (N)
h	average surface heat transfer coefficient of the filament ($W/m^2 \cdot K$)
k	thermal conductivity of melt (W/m · K)
k_0	thermal conductivity of air (W/m · K)
$R(z)$	filament radius at point z (m)
T	temperature (K)
T_a	ambient temperature (K)

T_{spin}	spinning temperature (K)
v_r	radial velocity (m/s)
v_z	axial velocity (m/s)
W	total mass flow rate (kg/s)
β	elongational viscosity (Pa · s)
ζ	dimensionless axial coordinate
θ	dimensionless temperature
ν_0	kinematic viscosity of air (m^2/s)
ξ	dimensionless radial coordinate
ρ	density (kg/m^3)

References

1. M. M. Denn, *Annu. Rev. Fluid Mech.*, **12**, 365 (1980).
2. E. H. Andrews, *Br. J. Appl. Phys.*, **10**, 39 (1959).
3. T. Matsuo and S. Kase, *J. Appl. Polym. Sci.*, **20**, 367 (1976).
4. S. Kase and T. Matsuo, *J. Polym. Sci. A.*, **3**, 2541 (1965).
5. S. Kase and T. Matsuo, *J. Appl. Polym. Sci.*, **11**, 251 (1967).
6. R. B. Bird, W. E. Stewart, and E. N. Lightfoot, *Transport Phenomena*, Wiley, New York, 1960.
7. D. U. von Rosenberg, *Methods for the Numerical Solution of Partial Differential Equations*, Farrar, Tulsa, 1969.

Received January 16, 1984
Accepted April 2, 1984